Available online at www.sciencedirect.com

SciVerse ScienceDirect

Acta Materialia 59 (2011) 7003–7009

Acta MATERIALIA

www.elsevier.com/locate/actamat

A dislocation density-based crystal plasticity constitutive model for prismatic slip in α-titanium

Alankar Alankar [a,b,*], Philip Eisenlohr [b], Dierk Raabe [b]

[a] *Materials Science Division, Los Alamos National Laboratory, MS-G755, Los Alamos, NM 87545, USA*
[b] *Max-Planck-Institut für Eisenforschung GmbH, Max-Planck-Straße 1, 40237 Düsseldorf, Germany*

Received 28 June 2011; received in revised form 22 July 2011; accepted 26 July 2011
Available online 22 August 2011

Abstract

A new constitutive plasticity model for prismatic slip in hexagonal α-titanium is developed. In the concept pure edge and screw dislocation densities evolve on the $\{1\,0\,\bar{1}\,0\}\langle 1\,\bar{2}\,1\,0\rangle$ slip systems. The model considers that the screw dislocation segments have a spread out core, leading to a much higher velocity of edge compared with screw dislocations. This enables the model to describe the observed transition in strain hardening from stage I to stage II in single crystals oriented for prismatic slip. Good agreement is found between the experimentally observed and simulated stress–strain behavior.

Keywords: Titanium; Crystal plasticity; Single crystal; Dislocations

1. Introduction

Prismatic slip (slip on the $\{1\,0\,\bar{1}\,0\}$ planes in the $\langle 1\,\bar{2}\,1\,0\rangle$ direction) is one of the dominant modes of plastic deformation in α-titanium [1–3]. Experimental investigations on the prismatic slip behavior of α-titanium single crystals [4] show a resemblance to single slip modes in fcc single crystals, particularly in terms of the transition between the stage I and stage II strain hardening modes [5]. In α-titanium oriented for prismatic slip this behavior is due to different velocities of the edge and screw dislocation segments.

In the 1970s–1980s many researchers explored the mechanisms that may give rise to the different behavior of edge and screw dislocations and hence to the underlying strain hardening mechanism in α-titanium. Conrad [6] and Tanaka and Conrad [7] attributed this glide behavior to interactions of dislocations with interstitials. These authors correlated the Peierls stress τ_P linearly with $\sqrt{c}$, where c is the impurity concentration. Naka et al. [8] suggested that the strain hardening in prismatic slip mode is due to modification of the dislocation core structure by interstitial impurities, e.g. O and N. They showed that the stage I to stage II transition in prismatic glide can be attributed to the spread out core of screw dislocations. Interaction between dislocations and interstitial impurities as a deformation controlling mechanism in prismatic glide in α-titanium had been observed before [9–11]. More specifically, it was suggested by these works that the screw dislocation velocity in particular is affected by the impurity content of the material [9–11]. Screw dislocations that pertain to the prismatic slip families have a spread out core on pyramidal $\langle a\rangle$ slip systems leading to a very low velocity of screw dislocations compared with edge dislocations. The presence of a significant amount of lattice friction on screw dislocations is also confirmed by the core spread observed in atomistic simulations by Legrand [12] and Bacon and Vitek [13]. Sastry and Vasu [14], based on their determination of the activation enthalpy for a thermally activated mechanism, suggested that low temperature deformation in titanium could be governed by nucleation of kink pairs to overcome the Peierls energy barrier. A kink pair

* Corresponding author at: Materials Science Division, Los Alamos National Laboratory, MS-G755, Los Alamos, NM 87545, USA. Tel.: +1 505 695 5542; fax: +1 505 667 8021.
E-mail address: alankar@lanl.gov (A. Alankar).

1359-6454/$36.00 © 2011 Acta Materialia Inc. Published by Elsevier Ltd. All rights reserved.
doi:10.1016/j.actamat.2011.07.053

mechanism was proposed by Seeger and Schiller to model such effects of the screw dislocation velocity [15].

The yield stress for prismatic slip in pure α-titanium shows a strong temperature dependence in the lower temperature regime, namely between 75 and 400 K [4,7,8,16,17]. The microstructure of deformed crystals in this regime is characterized by long and straight segments of screw dislocations [8,18–20]. Naka and Lasalmonie [21] differentiated between two regimes in the micromechanical behavior under prismatic glide conditions. They defined domain 1 as a regime in which the flow stress is thermally activated but no edge dipoles are created, and domain 2 as a thermally activated regime (at around 300 K) where edge dipoles are formed which cause cross-slip of screw dislocations between prismatic planes and first order pyramidal planes. However, the temperature bounds of these activation regimes are not rigidly defined. This is due to the fact that in many alloys that were mechanically characterized in the literature the impurity concentration was not well defined or known. This point, particularly the different activation regimes, is discussed in the work of Tanaka and Conrad [9]. Naka and Lasalmonie [21] distinguished the mechanisms at 77 and 374 K, but at 300 K the behavior was still ambiguous. At 77 K there is no sign of cross-slip and, as observed by electron microscopy, all dislocations remain on the primary glide plane. In crystals oriented for deformation on prismatic slip systems cross-slip activity is reported to occur in stage III [4], where the true strain has reached a value of ~0.65. At 374 K the microstructure shows wavy slip lines and electron microscopy confirms the occurrence of cross-slip activity [21]. Using slip trace analysis, the above authors also found the cross-slip plane to be a first order pyramidal plane and one of the easiest to activate secondary slip planes. Cross-slip activity is reported in Naka and Lasalmonie [22] to occur frequently at temperatures above 300 K. In the present work we thus consider the temperature range up to 300 K to be a non-cross slip regime.

Polycrystal plasticity finite element models in conjunction with phenomenological viscoplastic constitutive laws, e.g. Salem et al. [23] and Balasubramanian and Anand [24], have been used to simulate α-titanium deformation textures. However, in order to better understand slip activity in titanium under complex boundary conditions on a sound mechanisms-oriented basis under consideration of individual dislocation properties and interactions a single crystal-based model is needed. In this work we propose such a model and claim that it not only reproduces the experimentally observed plastic deformation behavior of single crystals, specifically the stage I to stage II strain hardening transition, but also helps to understand the origin of this transition in terms of the differences between screw and edge dislocation segments. The explicit activation of twinning is not covered in the current model formulation, as we concentrate on explaining the stage I and II strain hardening regimes in terms of the underlying dislocation mechanisms. Twinning can be activated, although in the current model when also choosing an adequate orientation factor. It is, however, not relevant in understanding the subtleties associated with the stage I to stage II strain hardening transition.

2. Constitutive model

In this section we present a model for prismatic slip activity in α-titanium. Slip activity is modeled using a set of dislocation density-based rate equations and different constitutive laws that are used to describe the velocities of edge and screw dislocations.

2.1. Parameterization of the microstructure

The total dislocation density evolution is a net effect of dislocation density multiplication and annihilation. The total dislocation density is given by the total edge and screw type dislocation densities.

$$\rho^{\alpha} = \rho_e^{\alpha} + \rho_s^{\alpha} \tag{1}$$

where α represents a prismatic slip system, and e and s represent the edge and screw dislocation densities, respectively.

2.2. Deformation kinetics

The kinematics of shear rate on each slip system is given in terms of a generalized Orowan form. The total plastic shear strain rate is given by:

$$\gamma^{\alpha} = b^{\alpha}(\rho_e^{\alpha}\bar{v}_e^{\alpha} + \rho_s^{\alpha}\bar{v}_s^{\alpha})\mathrm{sign}(\tau^{\alpha}) \tag{2}$$

where $\bar{v}_e^{\alpha}$ and $\bar{v}_s^{\alpha}$ represent the edge and screw dislocation velocities, respectively. Edge dislocation segments whose velocities are not affected by interstitials and impurities are pinned at the forest dislocation segments. The screw dislocation segments are assumed to move via formation of kink pairs. The phenomenological constitutive equations of velocities are explained in the following section.

2.3. Edge dislocation velocity

For both edge and screw dislocations Arrhenius type equations for the velocity are used. The average velocity for edge dislocations is given by:

$$\bar{v}_e^{\alpha} = \bar{v}_{0,e}\exp\left[-\frac{F_0}{k_B T}\left(1-\left(\frac{|\tau^{\alpha}|}{\tau_{0,e}+S^{\alpha}}\right)^{pe}\right)^{qe}\right] \tag{3}$$

where $\bar{v}_{0,e}$ is a reference velocity, F_0 is the free energy of the activation of motion, k_B is Boltzmann's constant, $\tau_{0,e}$ is the lattice friction stress acting on edge dislocations, and T is the absolute temperature. p_e and q_e are material coefficients such that $0 \leqslant p_e \leqslant 1$ and $1 \leqslant q_e \leqslant 2$.

2.4. Screw dislocation velocity

The velocity of a screw dislocation segment is governed by thermally activated nucleation of kink pairs. It is given by [25–28]:

$$\bar{v}_s^{\alpha} = b^{\alpha}\frac{l^{\alpha}}{l_0}\frac{v_D}{l_0}\exp\left[-\frac{F_{kink,0}}{k_B T}\left(1-\left(\frac{|\tau^{\alpha}|}{\tau_P}\right)^{ps}\right)^{qs}\right] \quad (4)$$

where $\bar{v}_s^{\alpha}$ is the velocity of a straight screw dislocation segment l^{α}, l_0 is the critical length for kink pair nucleation, v_D is the Debye frequency, τ_P is the Peierls stress, and b^{α} is the magnitude of the Burgers vector. The term $v_D b/l_0$ describes the attempt frequency for kink pair formation and the term $l^{\alpha}b/l_0$ describes the number of competing sites for kink pair formation on the segment l^{α} [28,29]. Using this phenomenological description of the velocity of screw dislocations Monnet et al. [30] have successfully predicted the low hardening regime in pure Zr single crystals oriented for slip on prismatic planes alone. Dislocation dynamics simulations show similarities between the configuration of dislocations in the deformed microstructure and those observed by electron microscopy [8,18,19]. As mentioned in Section 1, the effect of the impurity content results in a spread of the screw dislocation core, therefore, no explicit treatment is given of the specific role of the impurity content in the present work. The effect of the impurity content in our model is incorporated via the lattice friction stress $\tau_{0,e}$ acting on edge dislocations and the Peierls stress τ_P acting on moving screw dislocations and the initial kink nucleation length l_0. For simplicity the velocity of the edge dislocation could in principle be described in the model as a multiple of the velocity of the screw dislocation (e.g. 1000 times) (see, for example, Monnet et al. [30]). Instead, we use explicit constitutive equations for the velocities of the edge and screw dislocations, so that the effect of forest hardening by edge dislocations is inherently included.

2.5. Forest hardening

The slip resistance S^{α} on slip system α is given by a modified Taylor type equation [31], as shown below. The equations used here are similar to those suggested by Arsenlis and Parks [32], except for the fact that we consider the hardening coefficients to depend on the interacting slip systems alone, and not on the type of dislocations that are affected.

$$S^{\alpha} = \mu b^{\alpha}\sqrt{\sum\nolimits_{\beta} g^{\alpha\beta}(\rho_e^{\beta}\mathbf{n}^{\alpha}\cdot\mathbf{t}^{\beta} + \rho_s^{\beta}\mathbf{n}^{\alpha}\cdot\mathbf{t}^{\beta})} \quad (5)$$

where μ is the shear modulus, $g^{\alpha\beta}$ is the latent hardening coefficient for slip systems α and β, and ρ^{β} is the forest dislocation density. The coefficients in this interaction matrix are chosen so that the hardening behavior generally reflects the salient features of the stress–strain response reported in the literature. The self-interaction coefficient is assumed to be lower than the latent hardening coefficient. Because of the negligible mobility of screw dislocations, they do not form a substantial fraction of stable junctions. On the other hand, edge dislocations, due to their high velocities, create stable junctions much more frequently. This has also been observed in dislocations dynamics simulations for Zr [30]. Eqs. (3) and (4) introduced above reflect these observations, namely that only edge dislocations interact with forest dislocations.

2.6. Average segment length

The average segment length of dislocations l^{α} on slip system α is given by [32,33]:

$$l^{\alpha} = \frac{\lambda}{\sqrt{\sum_{\beta}(\rho_e^{\beta}\mathbf{n}^{\alpha}\cdot\mathbf{t}_e^{\beta} + \rho_s^{\beta}\mathbf{n}^{\alpha}\cdot\mathbf{t}_s^{\beta})}} \quad (6)$$

where ρ_e^{β} and ρ_s^{β} are the edge and screw type dislocation densities, respectively, on a forest slip system β. $\mathbf{n}^{\alpha}$ is the glide plane normal and $\mathbf{t}_e^{\beta}$ and $\mathbf{t}_s^{\beta}$ are the tangent directions of edge and screw dislocations on the forest slip system. λ is a proportionality coefficient to correlate the average dislocation segment length with the mean free path of dislocations. For simplicity we assume this coefficient to be identical for edge and screw dislocations.

2.7. Dislocation multiplication and annihilation

The rates for multiplication and annihilation of edge and screw dislocations are adopted from the work of Arsenlis and Parks [32]: We describe the edge and screw dislocation densities through the expansion of dislocation loops. This means that the edge dislocation density increases due to moving screw dislocations and the screw dislocation density increases due to moving edge dislocations.

$$\rho_{e,gen}^{\alpha} = (\rho_s^{\alpha}\bar{v}_s^{\alpha})/l^{\alpha}, \quad \rho_{s,gen}^{\alpha} = (\rho_e^{\alpha}\bar{v}_e^{\alpha})/l^{\alpha} \quad (7)$$

Two dislocations of opposite sign annihilate each other when they come within a critical distance. The annihilation rates are given by:

$$\dot{\rho}_{e,ann}^{\alpha} = -\frac{1}{2}\rho_e^{\alpha^2}R_e^{\alpha}\bar{v}_e^{\alpha}, \quad \dot{\rho}_{s,ann}^{\alpha} = -\frac{1}{2}\rho_s^{\alpha^2}R_s^{\alpha}\bar{v}_s^{\alpha} \quad (8)$$

R_e^{α} and R_s^{α} are the critical distances for edge and screw type dislocations. These values quantify how far the respective dislocation segments travel through a field of randomly distributed dislocations of opposite sign before undergoing annihilation.

In the next section we present a discussion of the simulation results obtained for the deformation of α-titanium single crystals. Materials properties and model parameters are shown in Table 1.

3. Simulation results and discussion

The three prismatic slip systems are $(\bar{1}\,0\,1\,0)[\bar{1}\,2\,\bar{1}\,0]$, $(1\,\bar{1}\,0\,0)[\bar{1}\,\bar{1}\,2\,0]$ and $(0\,1\,\bar{1}\,0)[2\,\bar{1}\,\bar{1}\,0]$. To simulate the stress–strain behavior of single crystals we use only one finite element of brick type consisting of eight integration points. Periodic boundary conditions (PBC) are used along the x, y, and z directions. The z direction is identical to the tensile direction TD. The total uniaxial true strain for all simulations is 0.5. Fig. 1 shows the predicted

Table 1
Material constants and parameters for α-titanium in the current simulations.

Elastic constants [34]	C_{11}	162.2 GPa
	C_{33}	180.5 GPa
	C_{44}	46.7 GPa
	C_{12}	91.8 GPa
	C_{13}	68.8 GPa
Edge dislocation velocity	p_e	0.61
	q_e	1.31
	$\bar{v}_{0,e}$	100.0 m s^{-1}
	F_0	2.5 e^{-19} J $atom^{-1}$
	k_B	1.38 e^{-23} J K^{-1}
	$\tau_{0,e}$	30 MPa
	R_e^α	9.6 e^{-9} m
Screw dislocation velocity	q_s	0.757
	q_s	1.075
	$F_{kink,0}$ [14]	1.77 e^{-19} J $atom^{-1}$
	τ_P [14]	323 MPa
	l_0	10 e^{-9} m
	R_s^α	86.6 e^{-9} m
Slip system interaction	Self-hardening	0.10
	Latent hardening	0.12
Mean free path coefficient	λ	20.0

$\bar{v}_{0,e}$, the pre-exponential factor in the equation for velocity of edge dislocation; p_e and q_e, exponential coefficients in the equation for edge dislocation; p_s and q_s, exponential coefficients in the equation for edge dislocation; F_0, the activation energy for edge dislocation motion; $F_{kink,0}$, the activation energy for the motion of screw dislocations via kink pair formation; k_B; the Boltzmann constant; $\tau_{0,e}$, the lattice friction acting on the motion of edge dislocations; τ_P; the Peierls stress on screw dislocations; l_0, the critical kink nucleation length; R_s^α and R_s^α, the critical radii of interactions for edge and screw dislocations, respectively.

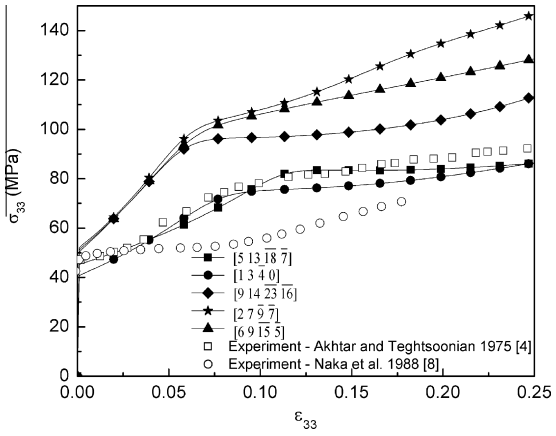

Fig. 1. Simulated stress–strain response in uniaxial tensile deformation in different prismatic orientations (cf. Table 1). Full symbols, simulation; open symbols, experiments.

Table 2
Crystallographic orientations for different single crystals used in the simulations.

Crystal	φ_1 (°)	Φ (°)	φ_2 (°)
$[5\ 13\ \overline{18}\ \bar{7}]\|\|TD$	20.5	101.6	17.0
$[1\ 3\ \bar{4}\ 0]\|\|TD$	164.6	90.0	15.3
$[9\ 14\ \overline{24}\ \overline{16}]\|\|TD$	156.9	113.3	23.0
$[2\ 7\ \bar{9}\ \bar{7}]\|\|TD$	168.1	115.7	11.8
$[6\ 9\ \overline{15}\ \bar{5}]\|\|TD$	157.3	101.3	22.6

TD, tensile direction.

stress–strain evolutions for different single crystals whose tensile axes are oriented for preferable deformation on prismatic slip planes. The initial orientations of the crystals are shown in Table 2. Fig. 1 also shows the experimental observations of Akhtar and Teghtsoonian [4] for a crystal whose tensile axis is oriented along the direction $[5\ 13\ \overline{18}\ \bar{7}]\|TD$. The second experimental observation is taken from Naka et al. [8] for a crystal which has its tensile axis oriented along $[1\ 3\ \bar{4}\ 0]\|TD$. Besides these stress–strain data not many other experiments have been published for α-titanium single crystals, particularly not as a function of crystal orientation, such as is required for direct comparison in this study. Also, the published single crystal experimental results reveal a strong dependence of the mechanical behavior on the impurity content, which makes it difficult to use them as a reference for the model.

The model shows good agreement with the experimentally determined stress–strain results of Akhtar and Teghtsoonian [4]. However, when using the same material parameters as for this single crystal (with tensile axis orientation $[5\ 13\ \overline{18}\ \bar{7}]\|TD$ [4]) for prediction of the stress–strain response of a sample with tensile axis $[1\ 3\ \bar{4}\ 0]\|TD$ the model does not match the experimental data well. We attribute this deviation to the oxygen content: the impurity content of α-titanium observed by these researchers in their material was $O^* = 120$ p.p.m. for the experiment with the $[5\ 13\ \overline{18}\ \bar{7}]\|TD$ axis and $O^* = 3270$ p.p.m. for that with the $[1\ 3\ \bar{4}\ 0]\|TD$ axis, respectively, where O^* represents the oxygen equivalent [8] of the total impurity content. As mentioned above, the impurity content is known to profoundly affect the stress–strain behavior in prismatic slip mode. Therefore, we conclude that the model is incapable of consistently predicting the stress–strain behavior of the two different crystals having $O^* = 3270$ p.p.m. in one case and $O^* = 120$ p.p.m. in the other case, using identical material parameters. For this purpose a composition-dependent model refinement would be required.

The stage I to stage II transition, which is a typical feature of the uniaxial stress–strain response of α-titanium single crystals oriented for deformation on prismatic slip systems, is well reproduced in all uniaxial deformation simulations. The strain at which the stage I to stage II transition occurs varies from a uniaxial strain of 0.05–0.12, depending on the crystallographic orientation of the crystal. In order to determine in more detail that the transition to stage II is indeed caused by the different edge and screw dislocation mobilities and not by the crystallographically originated activation of a secondary slip system (Schmid factor effect) the rotations of the tensile axis were tracked for all simulations. Fig. 2 shows the updated tensile axis orientation in the crystal reference frame with increasing uniaxial tensile deformation. The initial crystallographic

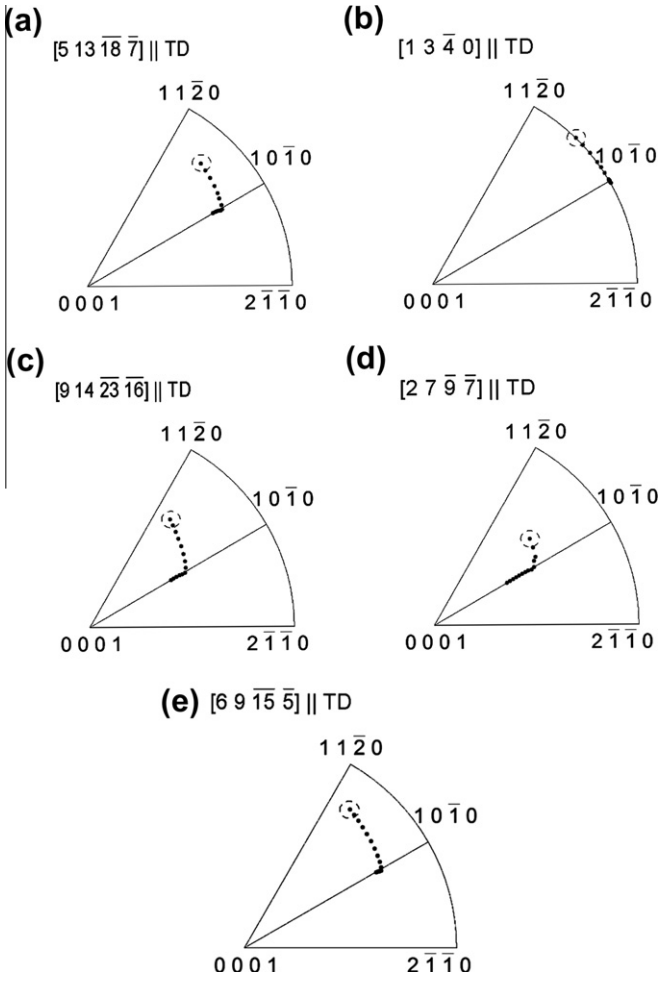

Fig. 2. Reorientation of the tensile axis in the crystal frame for prismatic oriented crystals. Initial orientations of the crystals are represented by the center of the dotted circles. The strain step between each tensile axis update is 0.05. *TD*, the tensile axis.

orientations of the crystals are represented by the centers of the dotted circles. For the following more detailed discussion we chose the case with the crystallographic orientation [5 13 $\overline{18}$ $\bar{7}$]||*TD*.

Fig. 3 reveals that the characteristic stress–strain behavior in prismatic glide is due to the different evolution and activation of edge and screw dislocations. Up to a strain of ~0.05 the crystal hardens via a single slip mode ($(\bar{1}\,0\,1\,0)[\bar{1}\,2\,\bar{1}\,0]$ slip system) and no latent hardening activity is noticed. At a strain of ~0.05 a secondary prismatic slip system ($(1\,\bar{1}\,0\,0)[\bar{1}\,\bar{1}\,2\,0]$ slip system) is activated and the screw dislocation density on this system increases rapidly. This effect is seen clearly in the evolution of the stress–strain response in terms of the transition from stage I to stage II. At the beginning of deformation edge dislocations start moving, i.e. the screw dislocation density starts increasing rapidly on the slip system $(\bar{1}\,0\,1\,0)[\bar{1}\,2\,\bar{1}\,0]$. Since these screw dislocation segments are created but do not move, there is no increase in the edge dislocation density as these dislocations move but do not multiply at this stage. Moreover, the rapid movement of edge dislocations causes

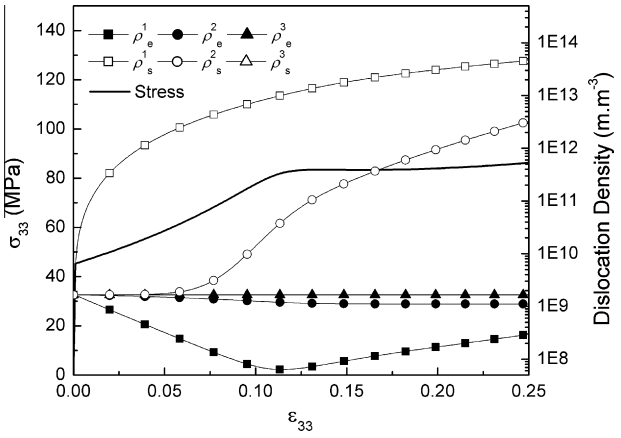

Fig. 3. Evolution of the edge and screw dislocation density as a function of uniaxial strain for orientation [5 13 $\overline{18}$ $\bar{7}$]||*TD* as predicted by the model. ρ^i_x represents the dislocation density of x type dislocations on slip system i. i represents slip systems 1, 2 and 3, i.e. $(\bar{1}\,0\,1\,0)[\bar{1}\,2\,\bar{1}\,0]$, $(1\,\bar{1}\,0\,0)[\bar{1}\,\bar{1}\,2\,0]$ and $(0\,1\,\bar{1}\,0)[2\,\bar{1}\,\bar{1}\,0]$.

a high rate of annihilation of these dislocations, which can be observed in Fig. 3 for the slip system $(\bar{1}\,0\,1\,0)[\bar{1}\,2\,\bar{1}\,0]$. Stage II starts with the evolution of screw dislocations on the slip system $(1\,\bar{1}\,0\,0)[\bar{1}\,\bar{1}\,2\,0]$. The multiplication of edge dislocations caused through the movement of screw dislocations on the primary slip system ($(\bar{1}\,0\,1\,0)[\bar{1}\,2\,\bar{1}\,0]$) starts at strains of ~0.12. The delay in the activation of edge and screw dislocations and, therefore, also in the transition from stage I to stage II in α-titanium as predicted by our model is consistent with the hypothesis of Naka et al. [8]. He suggested that the onset of stage I is governed by activation of edge dislocation motion on the primary slip system. Similarly, the onset of stage II is dominated by the activation of edge dislocation motion on the secondary slip system. It occurs due to the difference in lattice friction experienced by edge and screw dislocations [8].

As mentioned above in Section 1, the observation of long screw dislocation segments in α-titanium in the case of prismatic slip has been pointed out by many researchers in the past [8,21]. Similar observations have been reported for magnesium at 300 K, e.g. by Caillard and Couret [35]. A corresponding schematic image showing the expansion of a dislocation loop via kink pair formation is shown in Fig. 4. It is worth noting that the extent of anisotropy in the dislocation loops decreases with the onset of screw dislocation movement and, therefore, more interaction with forest dislocations occurs. The fact that in prismatic slip situations the stress–strain evolution is governed by screw dislocations is also supported by Figs. 5 and 6. The edge dislocation contribution to the total shear on any slip system is much higher at the beginning of deformation and the screw dislocations start contributing increasingly only at ~0.05 true strain. Edge and screw dislocation velocities increase with increasing strain on the non-primary slip systems (i.e. slip systems $(1\,\bar{1}\,0\,0)[\bar{1}\,\bar{1}\,2\,0]$ and $(0\,1\,\bar{1}\,0)[2\,\bar{1}\,\bar{1}\,0]$), while on the primary slip system $(\bar{1}\,0\,1\,0)[\bar{1}\,2\,\bar{1}\,0]$ the dislocation velocities decrease with increasing strain. The latter observation may

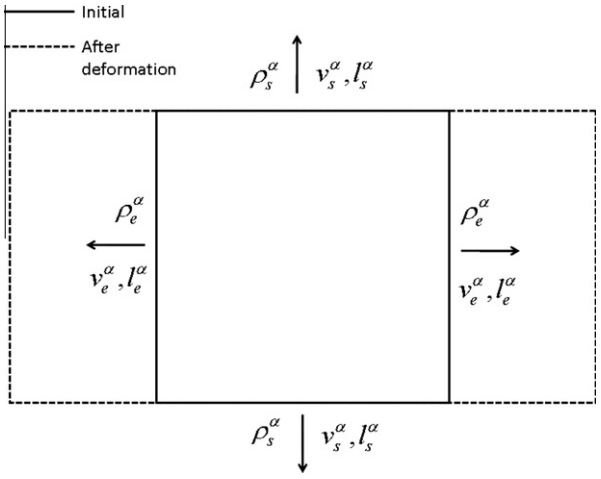

Fig. 4. Schmatic of the expansion of a dislocation loop due to different velocities of edge and screw dislocation. ρ_x^i, v_x^i, l_x^i represent the dislocation density, velocity, and segment length, respectively, for x type dislocations where x is edge or screw. i represents slip systems 1, 2 and 3, i.e. $(\bar{1}\,0\,1\,0)[\bar{1}\,2\,\bar{1}\,0]$, $(1\,\bar{1}\,0\,0)[\bar{1}\,\bar{1}\,2\,0]$ and $(0\,1\,\bar{1}\,0)[2\,\bar{1}\,\bar{1}\,0]$.

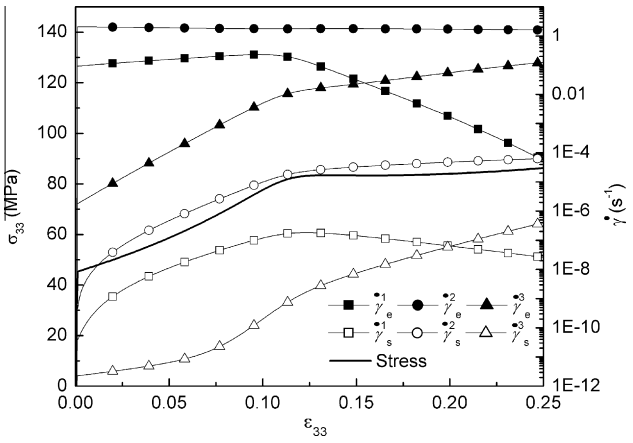

Fig. 5. Evolution of shear rate and uniaxial stress due to edge and screw type dislocations for orientation $[5\,13\,\overline{18}\,\bar{7}]\|TD$. $\dot{\gamma}_x^i$ is the shear rate due to x type dislocations. i represents slip systems 1, 2 and 3, i.e. $(\bar{1}\,0\,1\,0)[\bar{1}\,2\,\bar{1}\,0]$, $(1\,\bar{1}\,0\,0)[\bar{1}\,\bar{1}\,2\,0]$ and $(0\,1\,\bar{1}\,0)[2\,\bar{1}\,\bar{1}\,0]$.

be attributed to the fact that with higher shear activity on the primary slip system the dislocations undergo more interactions with forest dislocations. This leads to a decrease in the average dislocation velocity with increasing deformation. The model is able to reproduce these characteristic differences in the edge and screw segment velocities (cf. Fig. 6), which is essential to understand the stage I to stage II transition in α-titanium.

4. Conclusions

The crystal plasticity model presented here is based on thermally activated flow, multiplication and annihilation of dislocations. For these mechanisms the parameters were chosen based on the experimentally observed stress–strain behavior of α-titanium single crystals oriented for deformation on prismatic slip systems. The characteristic transition

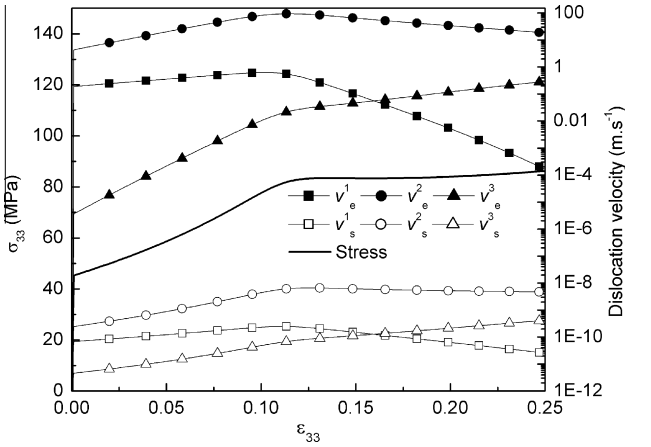

Fig. 6. Evolution of dislocation velocity as a function of uniaxial strain for crystals with the tensile axis along $[5\,13\,\overline{18}\,\bar{7}]\|TD$. v_x^i are dislocation velocities for x type dislocations where x = edge or screw. i represents slip systems 1, 2 and 3, i.e. $(\bar{1}\,0\,1\,0)[\bar{1}\,2\,\bar{1}\,0]$, $(1\,\bar{1}\,0\,0)[\bar{1}\,\bar{1}\,2\,0]$ and $(0\,1\,\bar{1}\,0)[2\,\bar{1}\,\bar{1}\,0]$.

of strain hardening from stage I to stage II is correctly predicted by the model. The transition is explained in terms of glide of dislocations via kink pair formation. It is shown that lattice friction on the screw dislocations due to spread-out cores plays a crucial role in the deformation of α-titanium oriented in prismatic slip mode. This dislocation density-based framework for modeling prismatic slip activity can be extended to other modes of slip activity in hexagonal crystal lattices. Such an extended model would enable the interaction between different modes of slip, i.e. prismatic, basal, pyramidal $\langle a\rangle$ and pyramidal $\langle c+a\rangle$, and would help to understand the phenomena associated with the spread-out cores in screw dislocations on other slip families in hexagonal crystals. Twinning could be incorporated via an adequate critical nucleation shear stress. This is important for full extension of the model since deformation on certain slip families, e.g. the basal slip family, is always accompanied by twinning [36]. A physically based single crystal plasticity model such as presented here would be ideal for the incorporation of dislocation density-based nucleation of twin, slip–twin interaction and slip assisted twinning activity in hcp metals [37–41].

The model presented here is the first approach to a crystal plasticity finite element model for hcp crystals which is based on dislocation densities and the mechanical behavior of individual single crystals. We do not include an explicit model for the effect of impurities. They can be incorporated by fitting the lattice friction stress that acts on the edge and screw dislocations.

Acknowledgements

The authors are grateful to the US National Science Foundation (NSF) and the Deutsche Forschungsgemeinschaft (DFG) for providing financial support for this work via the NSF Materials World Network Grant DMR-0710570 and the DGF Grant EI 681/2-1.

References

[1] Rosi FD, Dube CA, Alexander BH. Trans Metall Soc AIME 1953;197:257.
[2] Anderson EA, Jillson DC, Dunbar SR. Trans Metall Soc AIME 1953;197:1191.
[3] Churchman AT. Proc Roy Soc Lond Ser A Math Phys Sci 1954; 226: 216.
[4] Akhtar A, Teghtsoonian E. Metall Mater Trans A 1975;6:2201.
[5] Kocks UF. J Eng Mater Technol 1976;98:76.
[6] Conrad H. Acta Metall 1966;14:1631.
[7] Tanaka T, Conrad H. Acta Metall 1972;20:1019.
[8] Naka S, Lasalmonie A, Costa P, Kubin LP. Philos Mag A 1988;57:717.
[9] Tanaka T, Conrad H. Acta Metall 1971;19:1001.
[10] Soo P, Higgins GT. Acta Metall 1968;16:187.
[11] Mills D, Craig GB. Trans Metall Soc AIME 1968.
[12] Legrand PB. Philos Mag A 1985;52:83.
[13] Bacon DJ, Vitek V. Metall Mater Trans A 2002;33:721.
[14] Sastry DH, Vasu KI. Acta Metall 1972;20:399.
[15] Seeger A, Schiller P. Acta Metall 1962;10:348.
[16] Levine ED. Trans Metall Soc AIME 1966;236:1558.
[17] Biget MP, Saada G. Philos Mag A 1989;59:747.
[18] Cass TR. In: Jaffee RI, Promisel NE, editors. The science, technology and application of titanium: proceedings of an international conference organized by the Institute of Metals [and others] and held at the Royal Festival Hall, London, on 21–24 May, 1968. Oxford: Pergamon Press; 1970.
[19] Sakai T, Fine ME. Acta Metall 1974;22:1359.
[20] Farenc S, Caillard D, Couret A. Acta Metall Mater 1993;41:2701.
[21] Naka S, Lasalmonie A. Mater Sci Eng A 1982;56:19.
[22] Naka S, Lasalmonie A. J Mater Sci 1983;18:2613.
[23] Salem AA, Kalidindi SR, Semiatin SL. Acta Mater 2005;53:3495.
[24] Balasubramanian S, Anand L. Acta Mater 2002;50:133.
[25] Dorn JE, Rajnak S. Trans Metall Soc AIME 1964;230:1052.
[26] Guyot P, Dorn JE. Can J Phys 1967;45:983.
[27] Duesbery MS. Philos Mag A 1969;19:501.
[28] Tang M, Kubin LP, Canova GR. Acta Mater 1998;46:3221.
[29] Kubin LP, Devincre B, Tang M. J Comput-Aid Mater Des 1998;31.
[30] Monnet G, Devincre B, Kubin LP. Acta Mater 2004;52:4317.
[31] Franciosi P, Berveiller M, Zaoui A. Acta Metall 1980;28:273.
[32] Arsenlis A, Parks DM. J Mech Phys Solids 2002;50:1979.
[33] Akasheh F, Zbib HM, Ohashi T. Philos Mag A 2007;87:1307.
[34] Fisher ES, Renken C. J Phys Rev 1964;135:A482.
[35] Caillard D, Couret A. Mater Sci Eng A 2002;322:108.
[36] Akhtar A. Metall Mater Trans A 1975;6:1105.
[37] Capolungo L, Beyerlein I. J Phys Rev B Condens Matter Mater Phys 2008;78:024117.
[38] Wang J, Hoagland RG, Hirth JP, Capolungo L, Beyerlein IJ, Tomé CN. Scripta Mater 2009;61:903.
[39] Capolungo L, Beyerlein IJ, Tome CN. Scripta Mater 2009;60:32.
[40] Capolungo L, Beyerlein IJ, Kaschner GC, Tome CN. Mater Sci Eng A 2009;513–514:42.
[41] Bhattacharyya D, Cerreta EK, McCabe R, Niewczas M, Gray III GT, Misra A, et al. Acta Mater 2009;57:305.